

# Electronic structures of defective BN nanotubes under transverse electric fields

Shuanglin Hu,<sup>1</sup> Zhenyu Li,<sup>1</sup> X. C. Zeng,<sup>2</sup> and Jinlong Yang<sup>1,\*</sup>

<sup>1</sup>*Hefei National Laboratory for Physical Sciences at Microscale,  
University of Science and Technology of China,  
Hefei, Anhui 230026, People's Republic of China*

<sup>2</sup>*Department of Chemistry and Nebraska Center for Materials and Nanoscience,  
University of Nebraska-Lincoln, Lincoln, Nebraska 68588, USA*

(Dated: September 12, 2021)

## Abstract

We investigate the electronic structures of some defective boron nitride nanotubes (BNNTs) under transverse electric fields within density-functional theory. (16,0) BNNTs with antisite, carbon substitution, single vacancy, and Stone-Wales 5775 defects are studied. Under transverse electric fields, the band gaps of the defective BNNTs are reduced, similar to the pristine ones. The energy levels of the defect states vary with the transverse electric field directions, due to the different electrostatic potential shift at the defect sites induced by the electric fields. Therefore, besides electronic structure and optical property engineering, the transverse electric field can be used to identify the defect positions in BNNTs.

## I. INTRODUCTION

Boron nitride nanotubes (BNNTs) are wide-gap semiconductors regardless of their diameter, chirality, or the number of tube walls.<sup>1</sup> This implies that BNNTs own uniform electric and optical properties,<sup>2,3,4,5,6</sup> and makes BNNTs suitable for nanoscale electronic and optical applications. The external electric field is useful to tune the electronic properties of nano materials.<sup>7,8</sup> Khoo *et al.*<sup>8</sup> found that, when transverse electric fields are applied, pristine BNNTs show uniform gap closure behavior. Transverse electric fields can move the conduction band and valence band to two sides of the tubes. The band gaps of BNNTs are reduced almost linearly with the increase of electric fields. Under the same electric field, they are reduced with the increase of the diameter of BNNTs, independent of the chirality. The static dielectric response,<sup>9</sup> the screened polarizabilities,<sup>10</sup> and the optical properties of BNNTs under finite electric fields<sup>11</sup> have also been investigated by theoretical calculations. On the other hand, the electronic structures and properties of BNNTs can be modified by introducing intrinsic defects.<sup>12,13,14</sup> The intrinsic defects can introduce localized states in the band gap.<sup>12</sup> Defects and impurities can be used to obtain *n*-type or *p*-type semiconducting BNNTs.<sup>15,16</sup> The role of defects and also the role of polarization field in BNNTs have been reported.<sup>17</sup> However, to the best of our knowledge, it is still unclear how transverse electric fields affect the electronic structures of BNNTs with intrinsic defects.

In this work, we report the first-principles studies on the electronic structures of (16,0) BNNTs with antisite, carbon substitution, single vacancy, and Stone-Wales 5775 defects under transverse electric fields. Electric fields at three different directions perpendicular to the tube axis are applied.

## II. METHOD AND MODEL

Our electronic structure calculations are performed by means of the spin polarized density-functional theory implemented in Vienna *ab initio* simulation package (VASP).<sup>18,19</sup> The projector augmented wave (PAW)<sup>20</sup> method is used to describe the electron-ion interaction, and the cut-off energy is set to 400.0 eV. Perdew-Wang functional<sup>21</sup> is used for the generalized gradient approximation (GGA). The total energy is converged to  $10^{-5}$  eV. The atomic structures are fully relaxed without electric field until the forces are less than 0.01

eV/Å. The optimized geometrical structures are used to calculate the electronic structures under transverse static electric fields. Our test calculations on a (16,0) BNNT with B antisite indicate that geometry relaxation under electric field gives similar results.

We adopt (16,0) BNNTs with diameter 12.8 Å in our calculations. The tube axis is along the  $z$  direction. To minimize the interaction between adjacent images, we use a large cubic supercell ( $25.000 \times 25.000 \times 4.349$  Å<sup>3</sup>) for the pristine BNNT. For BNNTs with antisite and carbon substitution defects, we use a supercell with  $c=8.698$  Å, twice of the lattice parameter for the pristine BNNT. And for BNNTs with vacancies and Stone-Wales defects, we use a supercell with  $c=17.397$  Å. The special k-points for Brillouin Zone integrations are sampled using the Monkhorst-Pack scheme.<sup>22</sup> For the above three models,  $1 \times 1 \times 11$ ,  $1 \times 1 \times 7$ , and  $1 \times 1 \times 3$  k-points are chosen, respectively.

The method of applying static electric field implemented in VASP is in the spirit of the work of Neugebauer and Scheffler.<sup>23</sup> The electrostatic potential decreases along the direction of electric field. For convenience, all the defects are put at the positive  $x$  side in the supercell. The transverse electric field applied from the pristine side to the defective side is thus at the positive direction along  $x$  axis ( $\mathcal{E}_x$ ). And the effects of electric fields applied at the positive  $y$  direction ( $\mathcal{E}_y$ ) and negative  $x$  direction ( $\mathcal{E}_{-x}$ ) are also studied. The angle between the electric field and the positive  $x$  direction in the  $xy$  plane ( $\beta$ ) can be used to identify the direction of the electric field. The values of  $\beta$  for  $\mathcal{E}_x$ ,  $\mathcal{E}_y$ , and  $\mathcal{E}_{-x}$  are  $0^\circ$ ,  $90^\circ$ , and  $180^\circ$ , respectively. For (16,0) BNNTs, a large electric field is required to change the band structures significantly. The maximum strength of the applied electric fields in this study is  $0.3$  V/Å. The strength here is enough to induce distinct change of electronic properties of the tubes but no electron emission. It is expected that similar results should be obtained for larger BNNTs under weaker electric fields.

### III. RESULTS AND DISCUSSION

First, we examine the electronic properties of a pristine (16,0)BNNT under electric field. The pristine (16,0) BNNT is a semiconductor with a 4.47 eV band gap. The conduction band mainly comes from B atoms, and the valence band mainly comes from N atoms. When the electric field increases from 0.0 to 0.1, 0.2, and 0.3 V/Å, the band gap decreases from 4.47 eV to 4.04, 3.52, and finally 2.96 eV. It changes almost linearly with the increase of

electric field strength, which is consistent with the work of Khoo *et al.*<sup>8</sup>. The charge densities of the conduction band edge (CBE) states are moved along the direction of the electric field, to one side of the tube. And the valence band edge (VBE) states are moved to the opposite side of the nanotube.

We consider seven kinds of defects on the (16,0) BNNTs: boron antisite ( $B_N$ ), nitrogen antisite ( $N_B$ ), carbon substitution in a boron site ( $C_B$ ) or a nitrogen site ( $C_N$ ), boron vacancy ( $V_B$ ), nitrogen vacancy ( $V_N$ ), and Stone-Wales 5775 (SW). The results without electric field are presented first. The relaxed geometries are shown in Fig. 1. The formation energies presented in Table I are calculated as

$$E_{form} = E_{binding}[def-tube] - E_{binding}[ideal-tube], \quad (1)$$

where the  $E_{binding}[ideal-tube]$  and  $E_{binding}[def-tube]$  are binding energies of systems without and with defects, respectively. The results are a little larger than those in the (8,0) BNNT.<sup>13,14,24</sup> We also present work function of these BNNTs in the Table I. The band structures of the pristine and defective nanotubes are shown in Fig. 2, which are similar with the previous results.<sup>12</sup> The defect  $N_B$  introduces only occupied defect state,  $V_B$  introduces only unoccupied defect states, all the other defects introduce both unoccupied and occupied states in the band gap. In (16,0) BNNTs with  $C_N$  and  $B_N$ , the unoccupied defect states are close to the VBE, but farther than that in the  $V_B$  case. While in the tube with  $C_B$ , the occupied defect states are near to the CBE. The defect states in BNNTs with  $V_N$  and SW are deep in the band gap. The band structures of these systems can be sketched schematically in Fig. 3, we define the energy difference between the CBE and the VBE as  $E_{CV}$ ; the one between the lowest unoccupied defect state and the VBE as  $E_p$ ; and the one between the highest occupied defect state and the CBE as  $E_n$ . From Table II, we can see that, under zero electric field, the introduction of defects does not change the  $E_{CV}$ . As for the charge densities of the defect states, they are localized near the defect sites. It is shown from the profiles of the defect state charge densities in Fig. 4. For BNNTs with carbon substitution and single vacancy defects, there are also local magnetic moments in these systems (see Table III).

For the defective (16,0) BNNTs, we study the effects of the 0.3 V/Å electric fields at different directions. The  $E_{CV}$  in the defective systems are all reduced by the electric fields, with slight dependence on the field directions. In the narrowed band gap, the energy levels

of the defect states shift with the field directions remarkably, independent of whether the defect states are occupied or not. The  $\mathcal{E}_x$  lower the energy levels of the defect states. The  $\mathcal{E}_{-x}$  uplift the energy of the defect states. The energy levels of the defect states are between the above two cases, when  $\mathcal{E}_y$  is applied. As shown in Table II, when electric fields are applied, with the increase of the angle  $\beta$ , the relative movement of the defect states and the band edge states makes  $E_p$  increase and  $E_n$  decrease. In some defective systems, the lowest unoccupied defect state can be pushed into the conduction band by the electric fields, it makes the absence of the  $E_p$  in some cases in the Table II. And the highest occupied defect state can be also pushed into the valence band. The localized charge densities of these defects keep almost unchanged under electric fields. In Fig. 4, as an example, the profiles of the charge density of the lowest unoccupied defect state of the BNNT with  $B_N$  defect without and with  $0.3 \text{ V/\AA}$   $\mathcal{E}_{-x}$  are shown.

Although the energy levels of defect states move almost linearly with the increase of  $\beta$  in all cases, it affects the concentration of carriers differently, depending on the kind of defects. For BNNTs with  $V_B$  and  $C_N$  defects, the  $0.3 \text{ V/\AA}$   $\mathcal{E}_x$  results in a small  $E_p$  and enhances the  $p$ -type conductivity. The  $0.3 \text{ V/\AA}$   $\mathcal{E}_{-x}$  reduces the  $E_n$  and enhances the  $n$ -type conductivity most for the BNNT with  $C_B$  defect. In other situations, the  $E_p$  and  $E_n$  are maybe still too large to improve the conductivity significantly. However, we can use the change of conductivity under electric fields with different directions to identify the defect positions. If we change the directions of the transverse electric fields and measure the conductivity, for BNNTs with  $p$ -type carriers, when the electric field is applied from the pristine side to the defective side, we would get the max conductance. For BNNTs with  $n$ -type carriers, we can get the max conductance at the reversed field direction.

For the BNNTs with carbon substitution and single vacancy defects, the local magnetic moments show slight dependence on the field directions (see Table III), it can be related to the change of  $E_p$  or  $E_n$ . Especially, in the BNNT with  $V_B$  defect, when the electric fields are applied, with the increase of  $\beta$ , the magnetic moment is reduced. As shown in Fig. 2(b), in the band gap, there is one unoccupied defect state in the majority spin channel, and two in the minority spin channel. The reduction of  $E_p$  can increase the occupation probability on the lowest unoccupied defect state in the majority spin channel, so the total local spin can be increased, and the local magnetic moment can thus be enhanced. Other cases can be understood in a similar way. When the  $E_p$  and  $E_n$  are not so small, the magnetic moment

changes little with the electric field.

To understand the behavior of defect states under electric fields, we present an explanation based on the field induced electrostatic potential shift. When  $\mathcal{E}_x$  is applied, the defect is at the low potential side. While the field is reversed, the defect becomes at a relative high potential. So the electrostatic potential at the defect site can be related to  $\beta$ . If we take the center of the BNNTs as origin, at which the electrostatic potential is set to zero, the potential induced by electric fields at defect sites can be expressed as

$$\Delta P = -|\mathcal{E}| \times x \times \cos(\beta), \quad (2)$$

in which  $|\mathcal{E}|$  is the strength of the transverse electric field ( $0.3 \text{ V/\AA}$ ),  $x$  is the  $x$  coordinate of the defect site. As shown in Fig. 5, we examine the energy levels of the defect states and the band edge states with the  $\Delta P$  induced by electric fields, taking BNNTs with  $B_N$  and  $V_N$  defects as examples. The energy levels of the localized defect states are raised significantly with the increase of electrostatic potential at the defect sites. However, the levels of CBE and VBE are little affected compared to those of the defect states. The behavior of  $E_n$  and  $E_p$  under electric fields thus can be ascribed to the change of electrostatic potential at defect sites. And it can be expected that, stronger  $\mathcal{E}_x$  would bring down the electrostatic potential at the defect sites further, and reduce  $E_p$  more. The reversed stronger electric fields would reduce  $E_n$  similarly.

In most situations,  $E_{CV}$  is reduced to the value similar to the pristine BNNT under the electric field. But in some cases, the  $E_{CV}$  is unexpectedly large. Those are BNNTs with  $V_B$ ,  $C_N$ , and  $B_N$  under  $0.3 \text{ V/\AA}$   $\mathcal{E}_x$  and BNNTs with  $C_B$  under  $0.3 \text{ V/\AA}$   $\mathcal{E}_{-x}$ . The large  $E_{CV}$  is related to the corresponding small  $E_p$  or  $E_n$  in these cases. The small  $E_p$  or  $E_n$  enhances the metallicity of that system, and thus increases the screening. With the stronger screening, the reduction of electrostatic potential along the direction of electric field is slower, therefore,  $E_{CV}$  reduction is smaller. It can be seen from the profiles of  $yz$ -plane-averaged electrostatic potential under  $0.3 \text{ V/\AA}$   $\mathcal{E}_x$  and  $\mathcal{E}_{-x}$ , as shown in Fig. 6.

From the above results, we can see that, the electric fields can adjust the electronic structures of the defective BNNTs in a different way from pristine BNNTs. The transverse electric fields narrow the band gaps, move the defect states near to the VBE or CBE, and can change the conductive and optical properties smoothly. Under the same strength of electric fields, the quantities of  $E_p$  and  $E_n$  change monotonously with the increase of the

angle  $\beta$ . Compared to  $E_p$  and  $E_n$ , the  $E_{CV}$  changes little with  $\beta$ . So transverse electric fields can create shallow acceptor or donor states, depending on the kind of defects and the field directions. For one kind of defective BNNTs, one can measure the conductivity under different direction of electric fields, to identify the positions of the defects. The change of  $E_p$  and  $E_n$  under electric fields can also affect the local magnetic moments in the BNNTs with single vacancy and carbon substitution defects. The charge densities of the localized defect states are all almost unaffected by the electric fields. Besides changing their conductivity, the electric field engineering of the electronic structures of the defective BNNTs can also modify their optical properties. These external field tunable properties facilitate application of defective BNNTs as nano devices.

#### IV. CONCLUSION

In summary, we study the electronic structures of defective BNNTs under transverse electric fields. The band gaps of these BNNTs can be reduced by electric field like that in pristine BNNTs. The relative positions of the defect states in the band gap are moved when the transverse electric field direction is changed. The charge densities of localized defect states are not affected by the electric field. The behavior of electronic structures can be ascribed to the difference of the electrostatic potential induced by electric fields at the defect sites. Our results indicate that defective BNNTs can be used as electric field controlled nano electronic or optical devices.

#### ACKNOWLEDGMENTS

This work is partially supported by the National Natural Science Foundation of China (50121202, 20533030, 20628304), by National Key Basic Research Program under Grant No. 2006CB922004, by the Shanghai Supercomputer Center, the USTC-HP HPC project, and the SCCAS.

---

\* Corresponding author. E-mail: jlyang@ustc.edu.cn

<sup>1</sup> Rubio, A.; Corkill, J. L.; Cohen, M. L. *Phys. Rev. B* **1994**, *49*, 5081.

- <sup>2</sup> Radosavljević, M.; Appenzeller, J.; Derycke, V.; Martel, R.; Avouris, Ph.; Loiseau, A.; Cochon, J.-L.; Pigache, D. *App. Phys. Lett.* **2003**, *82*, 4131.
- <sup>3</sup> Lauret, J. S.; Arenal, R.; Ducastelle, F.; Loiseau, A.; Cau, M.; Attal-Tretout, B.; Rosencher, E. *Phys. Rev. Lett.* **2005**, *94*, 037405.
- <sup>4</sup> Arenal, R.; Stéphan, O.; Kociak, M.; Taverna, D.; Loiseau, A.; Colliex, C. *Phys. Rev. Lett.* **2005**, *95*, 127601.
- <sup>5</sup> Wirtz, L.; Marini, A.; Rubio, A. *Phys. Rev. Lett.* **2006**, *96*, 126104.
- <sup>6</sup> Park, C. H.; Spataru, C. D.; Louie, S. G. *Phys. Rev. Lett.* **2006**, *96*, 126105.
- <sup>7</sup> O’Keeffe, J.; Wei, C. Y.; Cho, K. J. *Appl. Phys. Lett.* **2002**, *80*, 676.
- <sup>8</sup> Khoo, K. H.; Mazzoni, M. S. C.; Louie, S. G. *Phys. Rev. B* **2004**, *69*, 201401(R).
- <sup>9</sup> Guo, G. Y.; Ishibashi, S.; Tamura, T.; Terakura, K. *Phys. Rev. B* **2007**, *75*, 245403.
- <sup>10</sup> Wang, L.; Lu, J.; Lai, L.; Song, W.; Ni, M.; Gao, Z. X.; Mei, W. N. *J. Phys. Chem. C* **2007**, *111*, 3285.
- <sup>11</sup> Chen, C. W.; Lee, M. H.; Lin, Y. T. *Appl. Phys. Lett.* **2006**, *89*, 223105.
- <sup>12</sup> Schmidt, T. M.; Baierle, R. J.; Piquini, P.; Fazzio, A. *Phys. Rev. B* **2003**, *67*, 113407.
- <sup>13</sup> Shevlin, S. A.; Guo, Z. X. *Phys. Rev. B* **2007**, *76*, 024104.
- <sup>14</sup> Gou, G. Y.; Pan, B. C.; Shi, L. *Phys. Rev. B* **2007**, *76*, 155414.
- <sup>15</sup> Xiang, H. J.; Yang, J. L.; Hou, J. G.; Zhu, Q. S. *Appl. Phys. Lett.* **2005**, *87*, 243113.
- <sup>16</sup> Zhi, C. Y.; Bando, Y.; Tang, C. C.; Golberg, D. *Phys. Rev. B* **2006**, *74*, 153413.
- <sup>17</sup> (a) Zhang, J.; Loh, K. P.; Yang, S. W.; Wu, P. *Appl. Phys. Lett.* **2005**, *87*, 243105. (b) Zhang, J.; Loh, K. P.; Deng, M.; Sullivan, M. B.; Zheng, J. W.; Wu, P. *J. Appl. Phys.* **2006**, *99*, 104309.; (c) Zhang, J.; Loh, K. P.; Zeng, J. W.; Sullivan, M. B.; Wu P. *Phys. Rev. B* **2007**, *75*, 245301.
- <sup>18</sup> Kresse, G.; Hafner, J. *Phys. Rev. B* **1993**, *47*, 558.
- <sup>19</sup> Kresse, G. Joubert, D. *Phys. Rev. B* **1996**, *59*, 1758.
- <sup>20</sup> Blochl, P. E. *Phys. Rev. B* **1994**, *50*, 17953.
- <sup>21</sup> Perdew, J. P.; Wang, Y. *Phys. Rev. B* **1992**, *45*, 13244.
- <sup>22</sup> Monkhorst, H. J.; Pack, J. D. *Phys. Rev. B* **1976**, *13*, 5188.
- <sup>23</sup> Neugebauer, J.; Scheffler, M. *Phys. Rev. B* **1992**, *46*, 16067.
- <sup>24</sup> Wu, X. J.; Yang, J. L.; Hou, J. G.; Zhu, Q. S. *J. Chem. Phys.* **2006**, *124*, 054706.

TABLE I: The formation energies ( $E_{form}$ ) and work function ( $\Phi$ ) of seven kinds of defects on the wall of the (16,0) BN nanotubes.

	$B_N$	$N_B$	$C_B$	$C_N$	$V_B$	$V_N$	SW
$E_{form}(eV)$	5.37	7.34	2.70	1.55	16.08	12.01	5.71
$\Phi(eV)$	4.86	3.91	2.58	5.33	5.74	3.76	4.81

TABLE II: The values of  $E_{CV}$ ,  $E_p$ , and  $E_n$  as plotted in Fig. 3 of pristine and seven kinds of defective (16,0) BNNTs under zero and 0.3 V/Å electric fields. The electric field is applied at positive  $x$ ,  $y$ , and negative  $x$  direction, respectively.

Electric field	$E_{CV}(eV)$				$E_p(eV)$				$E_n(eV)$			
	0	$\mathcal{E}_x$	$\mathcal{E}_y$	$\mathcal{E}_{-x}$	0	$\mathcal{E}_x$	$\mathcal{E}_y$	$\mathcal{E}_{-x}$	0	$\mathcal{E}_x$	$\mathcal{E}_y$	$\mathcal{E}_{-x}$
pristine	4.47	2.96	2.96	2.96	-	-	-	-	-	-	-	-
$N_B$	4.44	2.94	2.98	3.02	-	-	-	-	3.21	-	2.42	1.51
$V_B$	4.45	4.03	3.26	2.90	0.55	0.17	0.25	0.66	-	-	-	-
$C_N$	4.46	3.74	3.07	2.91	0.99	0.23	0.44	1.16	4.08	-	-	2.41
$B_N$	4.46	3.31	3.00	2.92	1.81	0.48	1.16	2.03	4.01	-	-	2.29
$C_B$	4.47	2.98	3.03	3.48	3.80	2.21	-	-	1.37	1.47	0.63	0.24
$V_N$	4.47	3.04	2.99	2.94	2.69	1.11	2.01	2.86	2.65	2.79	1.85	0.96
SW	4.43	2.85	2.96	3.01	3.82	2.20	-	-	4.12	-	-	2.46

TABLE III: The magnetic moments per cell ( $M$ ) of (16,0) BNNTs with  $C_B$ ,  $V_B$ ,  $C_N$ , and  $V_N$  defects under zero and 0.3 V/Å electric fields.

$M(\mu_B)$	0	$\mathcal{E}_x$	$\mathcal{E}_y$	$\mathcal{E}_{-x}$
$C_B$	1.00	1.00	0.99	0.90
$V_B$	1.04	1.41	1.27	1.02
$C_N$	0.99	0.87	0.97	0.99
$V_N$	1.00	1.00	1.00	1.00

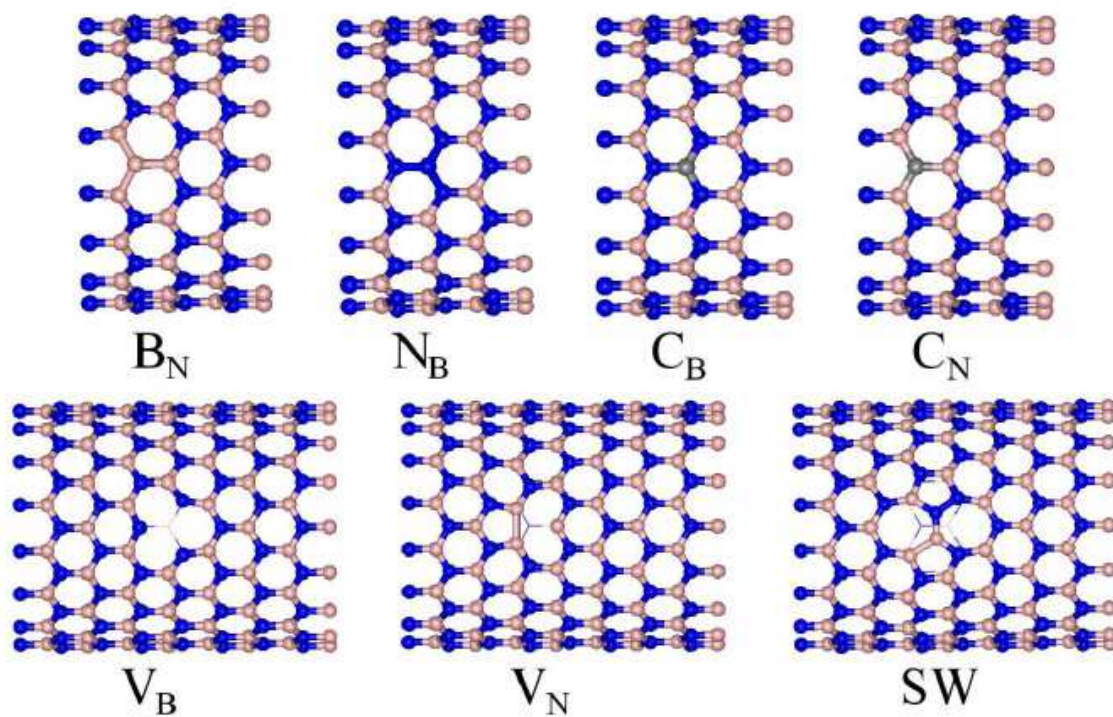


FIG. 1: The optimized structure of BNNTs with defects. Pink ball is boron, blue ball is nitrogen, and carbon is in gray.

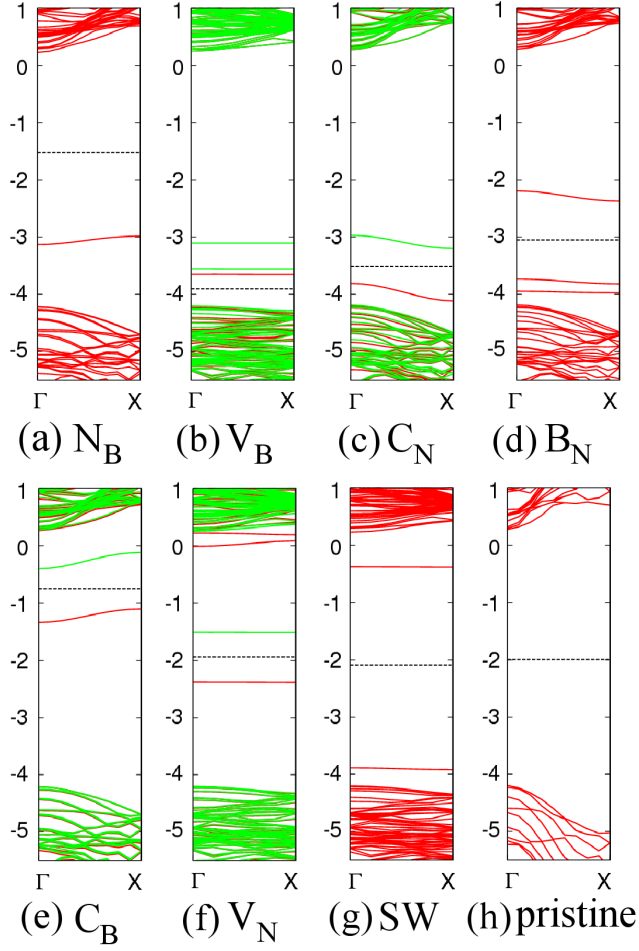


FIG. 2: Band structures of BNNTs with defects (a)  $N_B$ , (b)  $V_B$ , (c)  $C_N$ , (d)  $B_N$ , (e)  $C_B$ , (f)  $V_N$ , (g) SW and (h) pristine BNNTs without electric field. The red is the majority spin channel, and green is the minority spin channel. The dash line represents the fermi energy.

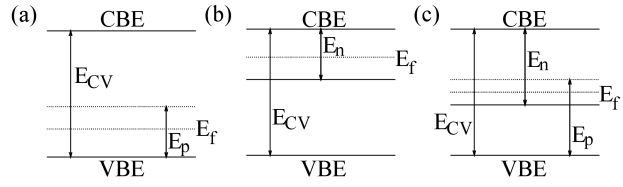


FIG. 3: The schematic diagram of the energy gaps between the defect states and the band edge states.  $E_{CV}$  is the gap between the conduction band and valence band edge states;  $E_p$  is the gap between the lowest unoccupied defect state and the valence band edge state; and  $E_n$  is the gap between the highest occupied defect state and the conduction band edge state.  $E_f$  is the fermi energy.

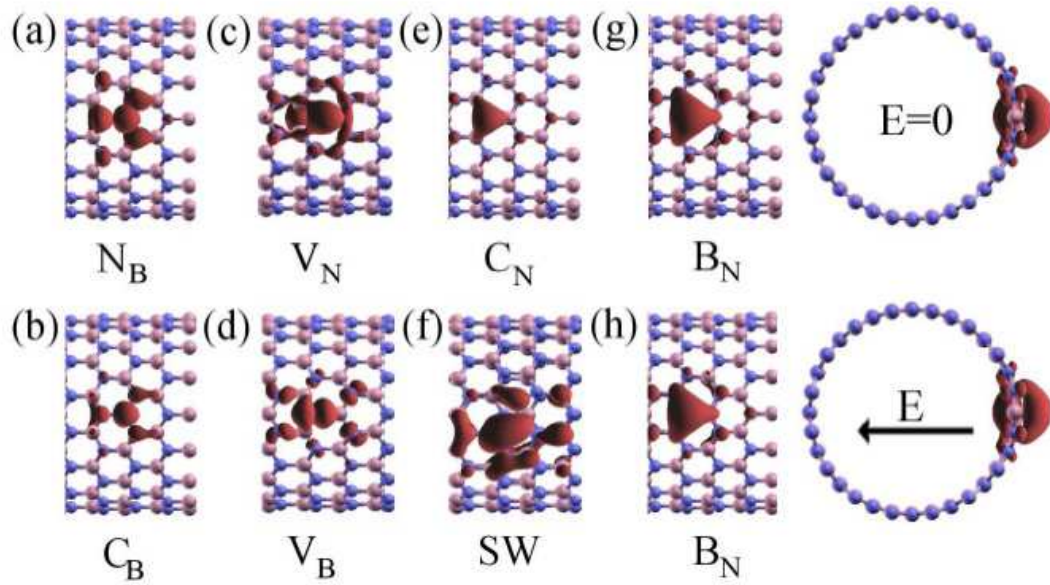


FIG. 4: The profiles of the  $\Gamma$  point charge densities of the highest occupied defect states of BNNTs with (a)  $N_B$ , (b)  $C_B$ , and (c)  $V_N$ ; and the lowest unoccupied defect states of BNNTs with (d)  $V_B$ , (e)  $C_N$ , and (f) SW under zero electric field. The axial view and side view of the lowest unoccupied defect state of BNNT with  $B_N$  (g) under zero electric field and (h)  $0.3 \text{ V/\AA } \mathcal{E}_{-x}$  are also presented.

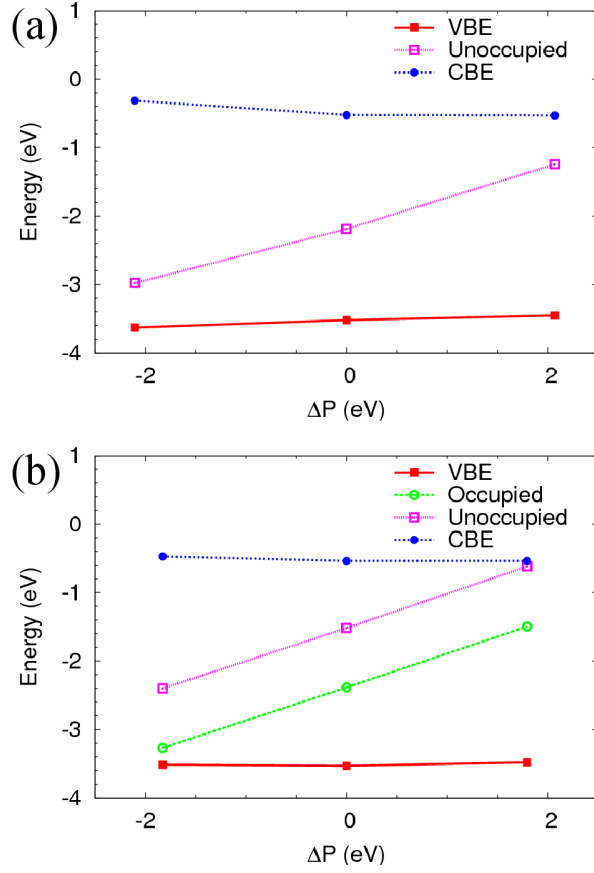


FIG. 5: The energy levels of the valence band edge (VBE) state, the occupied or unoccupied defect states, and the conduction band edge (CBE) state of BNNTs with (a)  $B_N$  and (b)  $V_N$  defects. The abscissa is the the shift of electrostatic potential at the defect sites induced by electric fields, calculated with Eq. 2. The strength of applied electric fields is  $0.3 \text{ V}/\text{\AA}$ .

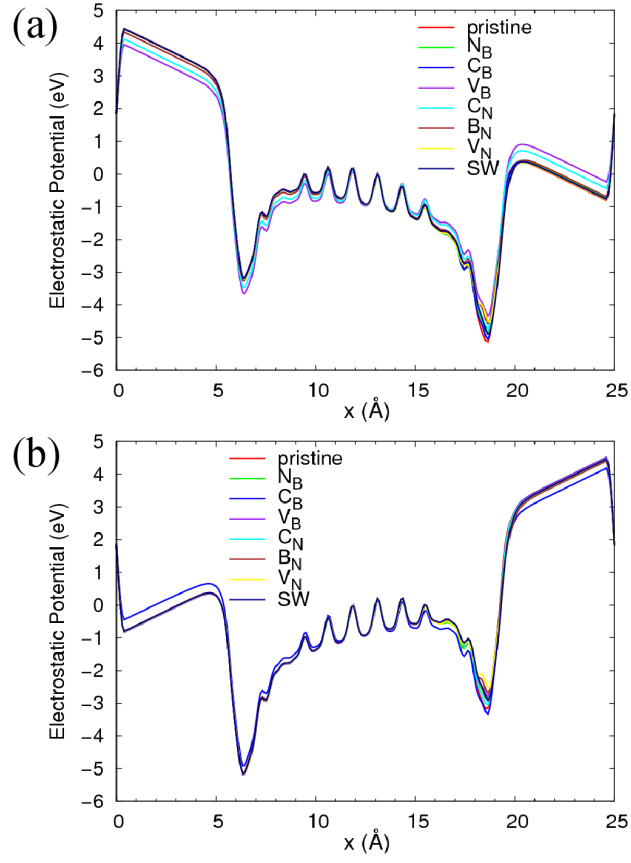


FIG. 6: The profiles of  $yz$ -plane-averaged electrostatic potentials of pristine and seven defective BNNTs under (a)  $\mathcal{E}_x$  and (b)  $\mathcal{E}_{-x}$ .